

The Plant Journal (2020) 104, 828-838

doi: 10.1111/tpj.14949

TECHNICAL ADVANCE

Optimization of multiplexed CRISPR/Cas9 system for highly efficient genome editing in *Setaria viridis* • •

Trevor Weiss^{1,2,3,4}, Chunfang Wang^{1,2,3,4}, Xiaojun Kang^{1,2,3,4}, Hui Zhao⁵, Maria Elena Gamo^{2,3,4,6}, Colby G. Starker^{2,3,4,6}, Peter A. Crisp^{1,2,3,†}, Peng Zhou^{1,2,3}, Nathan M. Springer^{1,2,3} , Daniel F. Voytas^{2,3,4,6} and Feng Zhang^{1,2,3,4,*}

Received 1 April 2020; revised 14 July 2020; accepted 21 July 2020; published online 12 August 2020.

SUMMARY

In recent years, Setaria viridis has been developed as a model plant to better understand the C4 photosynthetic pathway in major crops. With the increasing availability of genomic resources for S. viridis research, highly efficient genome editing technologies are needed to create genetic variation resources for functional genomics. Here, we developed a protoplast assay to rapidly optimize the multiplexed clustered regularly interspaced short palindromic repeats (CRISPR)/CRISPR-associated (Cas9) system in S. viridis. Targeted mutagenesis efficiency was further improved by an average of 1.4-fold with the exonuclease, Trex2. Distinctive mutation profiles were found in the Cas9 Trex2 samples, with 94% of deletions larger than 10 bp, and essentially no insertions at all tested target sites. Further analyses indicated that 52.2% of deletions induced by Cas9 Trex2, as opposed to 3.5% by Cas9 alone, were repaired through microhomology-mediated end joining (MMEJ) rather than the canonical non-homologous end joining DNA repair pathway. Combined with a robust Agrobacterium-mediated transformation method with more than 90% efficiency, the multiplex CRISPR/Cas9 -Trex2 system was demonstrated to induce targeted mutations in two tightly linked genes, svDrm1a and svDrm1b, at a frequency ranging from 73% to 100% in T0 plants. These mutations were transmitted to at least 60% of the transgene-free T1 plants, with 33% of them containing bi-allelic or homozygous mutations in both genes. This highly efficient multiplex CRISPR/Cas9_Trex2 system makes it possible to create a large mutant resource for S. viridis in a rapid and high throughput manner, and has the potential to be widely applicable in achieving more predictable and deletion-only MMEJ-mediated mutations in many plant species.

Keywords: Cas9, CRISPR, multiplexed genome editing, NHEJ and MMEJ DNA repair, *Setaria viridis*, *Trex2* exonuclease, technical advance.

INTRODUCTION

Setaria viridis (green foxtail) is an annual diploid C4 panicoid grass with a small genome and the wild relative to Setaria italica (foxtail millet), an agriculturally important crop in parts of Africa and Asia (Lata et al., 2013). Although historically regarded as an invasive weed, S. viridis has recently been developed as an emerging monocot model

species to investigate bioenergy feedstocks and panicoid food crops, such as maize, sorghum, sugarcane and switchgrass, and to better dissect the cellular and biochemical mechanisms of C4 photosynthesis (Brutnell *et al.*, 2010). Setaria viridis has many features that make it an attractive model system, including a short life cycle,

¹Department of Plant and Microbial Biology, College of Biological Sciences, University of Minnesota, Minneapolis, MN 55108, USA,

²Center for Plant Precision Genomics, University of Minnesota, Minneapolis, MN 55108, USA,

³Microbial and Plant Genomics Institute, University of Minnesota, Minneapolis, MN 55108, USA,

⁴Center for Genome Engineering, University of Minnesota, Minneapolis, MN 55108, USA,

⁵Institute of Tropical Bioscience and Biotechnology & Hainan Key Laboratory for Biosafety Monitoring and Molecular Breeding in Off-season Reproduction Regions, Chinese Academy of Tropical Agricultural Sciences, Haikou, Hainan Province 571101, China, and ⁶Department of Genetics, Cell Biology and Development, University of Minnesota, Minneapolis, MN 55108, USA

^{*}For correspondence (e-mail: zhangumn@umn.edu).

[†]Present address: School of Agriculture and Food Sciences, The University of Queensland, Brisbane, QLD, 4072, Australia

compact stature, reproduction via self-pollination and the ability to generate a high number of seeds (Defelice, 2002; Brutnell et al., 2010). Furthermore, the expanding genetic and genomic resources, including diverse germplasm accessions, chemically induced mutant populations, high quality reference genome of the A10.1 variety and the resequenced genomes from more than 600 accessions, make it possible to conduct large-scale gene discovery and functional genomics in S. viridis (Bennetzen et al., 2012; Zhu et al., 2017; Huang et al., 2019). Lastly, as another key factor for a successful model plant system, an efficient Agrobacterium-mediated transformation method has been reported in S. viridis, indicating that it is amenable to genetic engineering techniques (Van Eck, 2018; Huang et al., 2019; Nguyen et al., 2020).

Genome editing has significant potential to expedite gene discovery and functional genomics. A key characteristic of current genome editing technologies is the use of programmable nucleases, such as meganucleases, zinc finger nucleases (ZFNs), transcriptional activator-like effector nucleases (TALENs) or clustered regularly interspaced short palindromic repeats (CRISPR)/CRISPR-associated (Cas9), to create double-stranded DNA breaks (DSBs, or singlestranded nicks in some applications) at targeted loci. The induced DSBs can be exploited to introduce a variety of genomic modifications, such as deletions, insertions and nucleotide substitutions, using one of two main DNA repair pathways: end joining or homology-directed repair (HDR). The end-joining pathways, including non-homologous end joining (NHEJ) and microhomology-mediated end joining (MMEJ), are mostly used to generate insertions/deletions (indels) at targeted sites, whereas the HDR pathway is employed to precisely incorporate desired sequences into targeted loci by copying genetic information from co-transformed donor templates (Chen et al., 2019).

In recent years, the CRISPR/Cas9 system has become the reagent of choice to achieve efficient genome editing in many plant and animal species as a result of its simplicity. robust activity, versatility and multiplexing capability (Yin et al., 2017). When adopted in a new plant species, however, the CRISPR/Cas9 system often requires considerable optimization in vector construction, transgene expression, tissue culture and transformation efficiency (Yin et al., 2017). Additional strategies have been employed to further improve mutagenesis efficiency. For example, it has been demonstrated that the use of plants with a deficiency in the NHEJ pathway, such as the Ku70/Ku80 and Ligase IV mutants, could significantly enhance the frequency of targeted mutagenesis (Qi et al., 2013). Moreover, the simultaneous expression of exonucleases, such as Trex2, with CRISPR/Cas9 has been shown to enhance the frequency of targeted mutagenesis up to 2.5-fold in tomato and barley (Čermák et al., 2017). As for improving the multiplexing capability of the CRISPR/Cas9 system, multiplex CRISPR guide RNA (gRNA) has been tested by expressing from a single polycistronic cassette by a single promoter. In this design, the gRNA cassettes can be separated by ribozyme sites, CRISPR system yersinia ribonuclease 4 (Csy4) recognition sites, or tRNA sequences, which are then processed to release individual mature gRNAs for targeting (Tsai et al., 2014; Xie et al., 2015). When used in a new species, however, these multiplexing systems also need to be tested and optimized as a result of varied processing efficacy (Minkenberg et al., 2017; Shiraki and Kawakami,

Although one example of the CRISPR/Cas9-mediated gene knockouts has been described in S. viridis, a highly efficient, multiplexed gene editing system has yet to be reported (Huang et al., 2019). In the present study, we developed a protoplast-based transient assay for rapidly testing and optimizing the multiplexed CRISPR/Cas9 system in S. viridis. This system was also used to test the strategy of co-expression of the Trex2 exonuclease to further improve targeted mutagenesis efficiency in S. viridis. Finally, the optimized system was validated in stable transgenic plants to achieve highly efficient and heritable knockouts in two tightly linked *S. viridis* genes. The applications of this highly efficient, multiplexed CRISPR/Cas9_Trex2 system were discussed with respect to creating a large genetic mutant resource for S. viridis and achieving unique mutations in plant species.

RESULTS AND DISCUSSION

Development of multiplexed gene editing using S. viridis protoplasts

We sought to develop a protoplast-based assay for quickly assessing the CRISPR/Cas9 system in S. viridis (Figure S1). Protoplasts were isolated from young leaves of 14-day-old S. viridis seedlings. Transformation efficiency was tested using the green fluorescent protein (GFP) reporter driven by two different promoters: the Cestrum vellow leaf curling virus (CmYLCV) promoter and the Ubiquitin 2 promoter from switchgrass (PvUbi2) (Figure S2a). Both constructs produced robust GFP expression in approximately 80% of protoplasts at 24 h post transformation (hpt) and with almost 100% frequency at 48 hpt (Figure S2b).

The S. viridis protoplast assay system was then used to test and optimize CRISPR/Cas9 constructs targeting endogenous S. viridis genes, the domains rearranged methylase 1a (Drm1a), domains rearranged methylase 1b (Drm1b), male sterile 26 (Ms26) and male sterile 45 (Ms45) genes, respectively (Figure 1). The coding sequences of each gene were obtained by BLAST searching (https://phyto zome.jgi.doe.gov/pz/portal.html#!info?alias=Org_Sviridis_er) the reference genome of S. viridis accession A10.1 with the sequences of their maize orthologs, zmDrm1a, zmDrm1b, zmMs26 and zmMs45 (Table S1). Targeted sequences were

additionally verified by Sanger sequencing in *S. viridis* accession ME034v, the plant variety used in the present study. CRISPR gRNAs were designed to target the 5' exons or the conserved domains in each gene using CRISPOR (Haeussler *et al.*, 2016). Each target site contains a restriction enzyme site overlapping the CRISPR/Cas9 cut site to facilitate the cleaved amplified polymorphic sequences (CAPS) assay for subsequent genotyping analysis (Figure 1).

To achieve multiplexed gene editing in *S. viridis*, we tested two polycistronic gRNA expression systems, the Csy4-based and the tRNA array-based systems, in protoplasts (Xie *et al.*, 2015; Čermák *et al.*, 2017). Constructs containing gRNAs targeting the *Drm1a* and *Drm1b* genes (Figure S3a) were each co-transformed with Cas9 plasmids into protoplasts. As depicted in Figure 2a, high indel mutation frequencies were observed at each target site, ranging from 46% to 82%, indicating that both Csy4 and tRNA-based systems worked effectively in *S. viridis* protoplasts.

The *Trex2* exonuclease enhances targeted mutagenesis with unique mutation profiles

We chose the tRNA-based system for multiplexed genome editing in S. viridis for further development as a result of its proven efficiency and simplicity (Xie et al., 2015; Minkenberg et al., 2017). The multiplexing gene editing constructs, pMG198 and pMG199, were made containing the Cas9 expression cassette and the gRNA array. Each construct contained two gRNA sequences that simultaneously targeted the Ms26 and Ms45 genes at the selected gRNA 1 or 2 sites, respectively (Figure S3b). When these constructs were tested in protoplasts, high indel mutation frequencies were observed at each target site using nextgeneration sequencing (NGS): 45-60% for the Ms26 gRNA1 and gRNA2 sites and 35-37% for the Ms45 gRNA1 and gRNA2 sites, respectively (Figure 2b). To test whether the mutagenesis efficiency can be further improved through co-expression of the *Trex2* exonuclease, these multiplexing

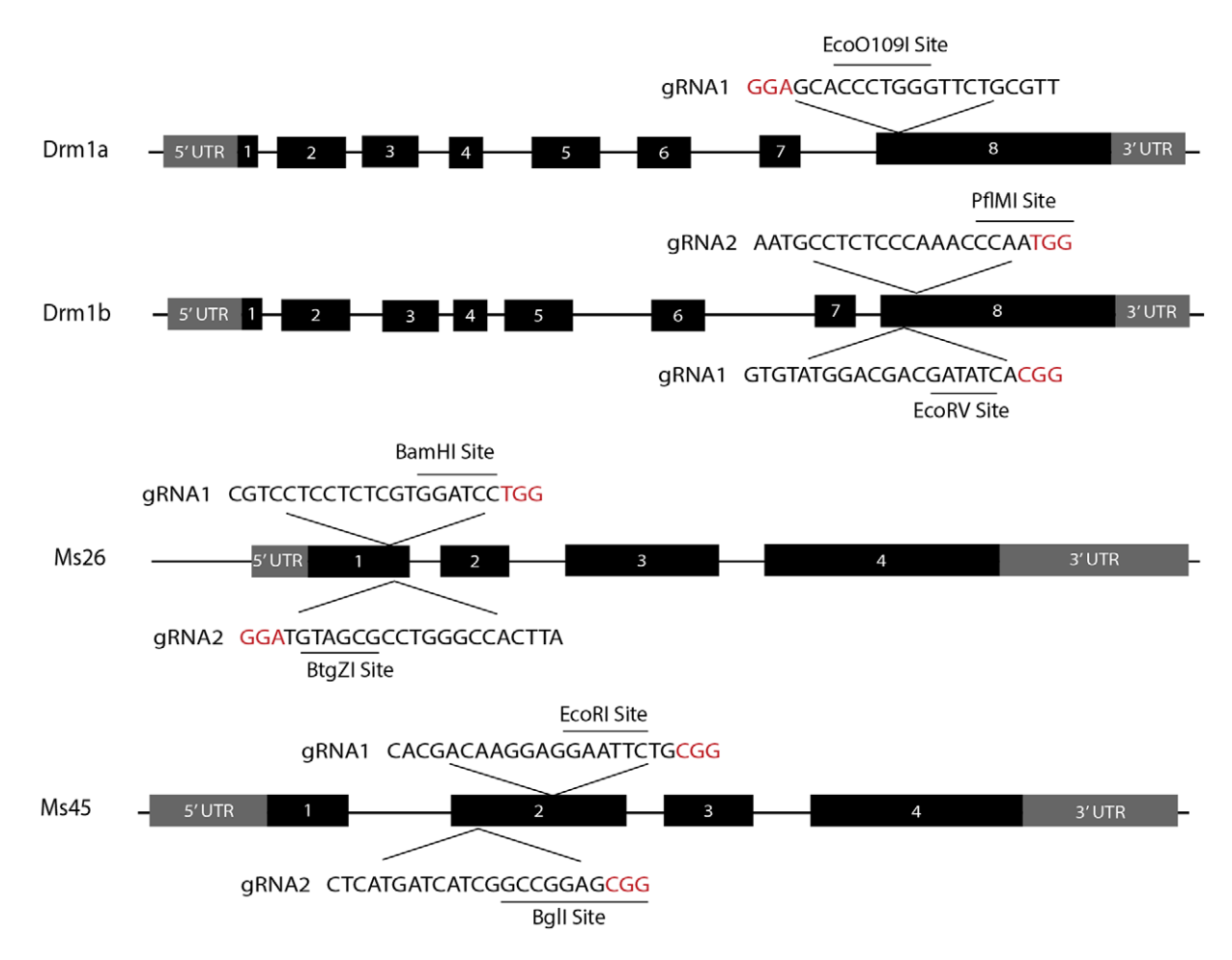


Figure 1. The schematic structures of the *Drm1a, Drm1b, Ms26* and *Ms45* genes. Each black box represents an exon, with gray boxes representing the 5' and 3' untranslated regions. Two guide RNAs (gRNAs) were designed to target *Drm1b, Ms26* and *Ms45*, with the distance between gRNAs being 114, 168 and 75 bp apart, respectively. Individual gRNA targeted sites are shown in each gene, with the restriction enzyme sites underlined and the protospacer adjacent motif (PAM) in red.

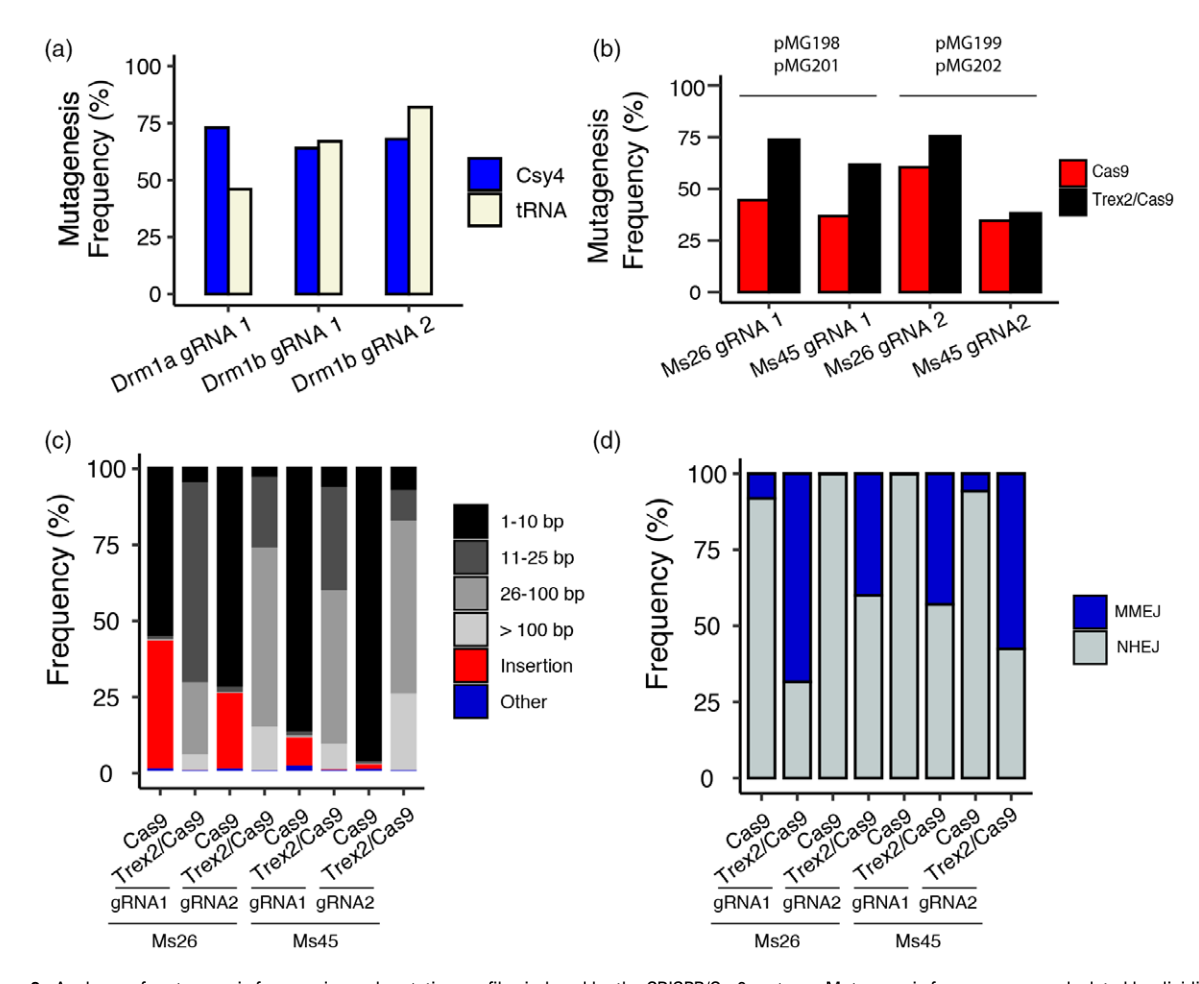


Figure 2. Analyses of mutagenesis frequencies and mutation profiles induced by the CRISPR/Cas9 systems. Mutagenesis frequency was calculated by dividing the total number of modified reads by the total number of reads. (a) Comparison of mutagenesis frequency mediated by the CRISPR system yersinia ribonuclease 4 (Csy4) (blue) and tRNA (beige) based guide RNA (gRNA) processing system. The gRNA sites, Drm1a gRNA 1 and Drm1b gRNAs 1 and 2, were targeted and analyzed by next-generation sequencing (NGS). (b) Comparison of mutagenesis frequency induced by Cas9 (red) and Cas9_Trex2 (black). The gRNA sites, Ms26 gRNA 1, Ms26 gRNA 2, Ms45 gRNA1 and Ms45 gRNA 2, were targeted and analyzed by NGS. (c) Comparison of mutation profiles induced by Cas9 and Cas9_Trex2. The stacked bar graph was generated for each gRNA targeted site with either Cas9 or Cas9_Trex2. The deletions are represented on a grayscale according to size, insertions are indicated in red and all other reads (i.e. substitutions, substitutions plus deletions and substitutions plus insertions) are indicated in blue. (d) Comparison of DNA repair outcomes induced by Cas9 and Cas9_Trex2. The frequencies of distinct DNA repair outcomes as either microhomology-mediated end joining (MMEJ) (blue) or nonhomologous end joining (NHEJ) (gray) were plotted in each sample with Cas9 or Cas9_Trex2.

CRISPR/Cas9 constructs were modified by cloning the *Trex2* coding sequences into the Cas9 expression cassette. The resulting Cas9_Trex2 plasmids, pMG201 and pMG202 (Figure S3b), were then transformed into protoplasts, respectively. At each target site, an average 1.4-fold increase in mutagenesis frequency, ranging from 1.1-fold to 1.7-fold, was observed from the samples with Trex2 as compared to those without Trex2 (Figure 2b). Thus, our results demonstrated that co-expression of the Trex2 exonucleases with CRISPR/Cas9 further improved mutagenesis frequency in S. viridis.

Increased deletion size was observed in tomato and barley when Trex2 was employed (Čermák et al., 2017). However, a thorough characterization of the mutations induced by the combination of Cas9 with the Trex2 exonuclease has yet to be reported using a large data set. In the present study, the mutation profiles were analyzed from a total of 516,815 NGS reads, and compared between the samples with and without co-expression of Trex2 (Table S2). In the samples without Trex2, both insertional and deletional mutations were observed in all four targeted sites, with 1.6-42.1% insertions, the majority of which were 1-bp insertions, and 57.1-97.8% deletions (Figure 2c). Among these deletions, 97.2-98.9% were smaller than 10 bp. Conversely, in the samples with Trex2, 94% of deletions, ranging from 92.3% to 96.6%, were larger than 10 bp, with 12% of them extending over 100 bp (Figure 2c). When they were further plotted along each targeted region, the deletions from the samples without Trex2 were found clustered in the 5' of the protospacer adjacent motif (PAM) sequences (PAM-distal regions) and within 10 bp of the DSB site. By contrast, the sequences from the four targeted

sites with *Trex2* contained much larger deletions that were symmetrically distributed on each side of PAM and that extended up to more than 100 bp (Figure S4). Additionally, it is worth noting that almost no insertions were observed in the samples with *Trex2* as opposed to up to 42.1% insertional mutations in those without *Trex2*. This finding suggested that the DNA breaks induced by Cas9_Trex2 could be repaired differently from those induced by Cas9 alone to prevent small insertions. Further investigations will be required to determine the underlying mechanisms.

Interestingly, in the samples with Trex2, some specific deletions appeared frequently, exemplified by the 48-bp deletions (3.5% of all deletions) in the Ms26 gRNA2 sample and the 87-bp deletions (7.4% of all deletions) in Ms45 gRNA 2 (Figure S5). Examination of these particular deletions uncovered 2, 3 and 4 bp microhomologies at the Ms26 gRNA 2 junction sites (Figure S6) and 2, 4, 5 and 6 bp microhomologies at the Ms45 gRNA 2 junction sites, indicating that the microhomology-mediated end joining pathway was involved in creating these deletions. Although previous studies have reported that Cas9-induced DSBs can be repaired through both NHEJ and MMEJ pathways, a recent study indicated that co-expression of *Trex2* with CRISPR/Cas9 predominately results in DSB repair via the NHEJ pathway in human cell lines (Bae et al., 2014; Ata et al., 2018; Taheri-Ghahfarokhi et al., 2018; Allen et al., 2018). To investigate the contribution of these two major end-joining pathways in our samples, over 150 000 NGS reads from the samples with and without co-expression of Trex2 were analyzed based on the presence/absence of microhomology at the deletion junction sites. As a result, in the samples with Trex2, a significant fraction of deletions, with an average of 52.2% (ranging from 39.9% to 68.4%) appeared to be repaired by MMEJ, whereas the samples without Trex2 exhibited an average of only 3.5% of deletions (ranging from 0.11% to 8.1%) repaired through MMEJ (Figure 2d).

The previous study by Chari *et al* (2015) suggested that *Trex2* could increase off-targeting mutation frequency in human cells and that careful gRNA design was crucial to reduce this risk. In the present study, the candidate gRNAs were selected using crispor, with the lowest off-targeting scores possible (Haeussler *et al.*, 2016). Four top-ranked off-target sites of *Ms26* gRNA1, two sites with 3-bp mismatches and two sites with 4-bp mismatches, were identified by crispor (Table S3). Each site was subjected to PCR amplification and NGS from the samples with and without *Trex2*, respectively. As a result, no significant mutation was detected at all four sites from any sample (Table S3). Although we cannot rule out the possibility that *Trex2* could increase off-targeting in plant cells, this finding confirmed that careful gRNA design is important to reduce the risk.

Taken together, our results indicate co-expression of the *Trex2* exonuclease with CRISPR/Cas9 can be used as a general strategy to increase the efficiency of targeted deletions in plants. In addition, the high frequency of the MMEJ events may also increase the predictability of the mutation outcomes, which is of particular value when precise deletional mutations are preferred. Although the mechanisms of how Trex2 improves Cas9-induced mutation frequency and promote MMEJ repair in plants remain to be clarified, this process likely involves at least two major steps. First, upon DSB induction at a target site, the Trex2 protein displaces the CRISPR/Cas9 complex, allowing for resectioning of the broken DNA ends in a 3' to 5' manner (Mazur and Perrino, 1999). Next, the resected ends are rejoined through either NHEJ or MMEJ repair pathway (Figure S7). As a result, the Trex2-mediated resectioning makes this DNA repair process more error prone and gives rise to higher mutation rates with larger deletions. It is not clear why Trex2 promotes MMEJ over NHEJ repair in S. viridis but not in human cells. These findings suggested that different organisms may invoke different end-joining pathways to repair the resected DSBs. Further investigations are needed to determine the underlying mechanisms.

Highly efficient multiplexed genome editing in T0 transgenic plants

The multiplex CRISPR/Cas9_Trex2 system tested with the protoplast assay was then used to create heritable mutations in the two linked Drm1 genes. Three T-DNA constructs were made by assembling the tRNA-gRNA array cassette with the Cas9 Trex2 cassette using the Golden Gate assembly method (Cermák et al., 2017). In these T-DNA vectors, the tRNA-gRNA array contained up to three gRNAs targeting the Drm1a and Drm1b genes individually or collectively (Figure S8a). Stable transgenesis was carried out using Agrobacterium-mediated transformation. In total, 85, 26 and 103 potential transgenic plants were regenerated from 86, 29 and 112 mature seed-derived calli in the transformation groups, pTW037, pTW044 and pTW045, respectively, exhibiting the high transformation efficiency (> 90%) for this S. viridis ME034v variety (Table 1). A subset of candidate plants was randomly picked from each group and further genotyped by genomic PCR using the primers for the hygromycin marker gene (Figure S8b). The presence of T-DNA constructs was confirmed in all 30 plants, indicating a very low escape rate in plant transformation. Notably, the overall transformation efficiency reported in the present study is significantly higher than those of previous studies, in the range 5-15% for the variety A10.1 (Van Eck et al., 2017; Nguyen et al., 2020). The difference between the observed transformation efficiencies could be attributed to the S. viridis variety, ME034v, as used in the present study. A similar transformation efficiency for ME034v was also observed in other studies (Zhu et al., 2017; Huang et al., 2019). Further investigations are required to determine the underlying mechanism(s) responsible for this difference in transformation efficiency.

11 (100%)

11 (100%)

11 (100%)

Table 1 Summary of T0 plant characterization

112

pTW045

Characterization of T0 plants								
T-DNA construct	Number of calli	Number of plants regenerated	Number of plants genotyped	Number of plants with mutations (frequency)				
				Drm1a (gRNA1)	Drm1b (gRNA1)	Drm1b (gRNA2)		
pTW037	86	85	8 (100%) [†]	NA	8 (100%)	NA		
pTW044	29	26	11 (100%) [†]	9 (82%)	NA	8 (73%)		

11 (100%)

Next, the transgenic plants were examined at the targeted regions using genomic PCR followed by a restriction enzyme digestion, namely the CAPS assay (Figure 3a; Figure S9). As summarized in Table 1, the frequency of plants with mutations induced by the single gRNA T-DNA construct, pTW037, was 100% in the Drm1a target site. Similarly, 82% and 73% of plants with the double gRNA T-DNA plasmid, pTW044, carried mutations in the Drm1a and Drm1b genes, and 100% of plants with the triple gRNA T-DNA construct, pTW045, had mutations in all three target sites (Figure 3a and Table 1). Accordingly, the multiplex CRISPR/Cas9_Trex2 system that was demonstrated to be highly efficient in the protoplast assay also induced high frequency mutagenesis in stable transgenic plants.

Inheritance of targeted mutations in T1 progenies

Plants with the triple gRNA T-DNA construct were further investigated to test the heritability of the mutations induced in T0 plants. The CAPS genotyping assay indicated that all 11 T0 plants contained mutations in all three targeted sites at variable frequencies (Figure 3a). To quantify the mutagenesis frequency in each T0 plant, PCR amplicons spanning each targeted region were sequenced using next-generation sequencing. Over 20 000 sequencing reads were generated from each PCR amplicon, and analyzed to estimate the indel mutation frequency. Consistent with the results from the CAPS genotyping assay, mutagenesis frequencies were observed in each T0 plant ranging from 3% to 99% in the Drm1a site, from 10% to 99% in the Drm1b gRNA1 site and from 11% to 99% in the Drm1b gRNA2 site, respectively (Figure 3b). In general, the mutagenesis frequencies were positively correlated across all three target sites. For example, four of 11 plants showing lower mutagenesis efficiency in the Drm1a target site (under 10%) also displayed lower mutagenesis efficiency in the two Drm1b target sites (Figure 3b).

Five T0 plants, 12, 15, 84, 86 and 94, showing mutation frequencies > 50% at all three targeted sites, were chosen to be self-pollinated and grown to maturity. Ten T1 progenies from each T0 plant were grown for further characterization. Using the CAPS genotyping assay, high frequencies of mutant plants were detected in these T1 populations,

ranging from 50% to 100%, 60% to 90% and 30% to 100% at three target sites, Drm1a, Drm1b gRNA1 and Drm1b gRNA2, respectively (Figure S10, Table 2). To further distinguish heritable mutations from somatic mutations in these T1 plants, a genomic PCR was conducted to identify T-DNA transgene-free plants using primers for the hygromycin marker gene (Figure S11, Table S4). Because the hygromycin marker gene is close to the left border (LB) region of the T-DNA, to rule out the possible presence of partial T-DNA sequences (Collier et al., 2018), the T1 plants were also subjected to the luciferase assay to detect the expression of the luciferase reporter gene close to the right border (RB) region. Lack of a fluorescence signal further confirmed the absence of T-DNA sequences in the T1 plants (Figure S12). As a result, four of five T1 populations, 12, 15, 84 and 86, exhibited segregation of the transgene (Table 2). Of 50 T1 plants, 10 transgene-free plants were identified (Table 3, Table S4). Among the transgene-free plants, six (60%) showed mutations in at least one of the three target sites, with one plant (10%) having a mutation at two target sites and two plants (20%) having mutations at all three target sites (Table 3). Two transgene-free plants, 12-1 and 12-9, with mutations in all three target sites were further characterized by NGS (Table 3). As shown in Figure 3c, both NHEJ and MMEJ-mediated deletions were recovered in these two mutant plants (Figure 3c). Notably, although the CAPS assay suggested that heterozygous mutations occurred at the DRM1b gRNA2 site in these plants (Figure S11), the NGS data revealed bi-allelic mutations in both plants. Close examination of these mutations identified a 1-bp deletion at this target site that did not disrupt the restriction enzyme (PfIMI) recognition site used in the CAPS assay. This finding suggested that the CAPS assay used to screen the T1 plants may underestimate the mutagenesis frequency transmitted to the T1 populations. Taken together, these results clearly demonstrated that the mutations are transmissible in the S. viridis mutant plants at high efficiency. This made it possible to recover homozygous mutants from a relatively small population of T1 plants and to generate multiple gene knockout events simultaneously and rapidly, which is particularly of value with respect to editing tightly linked genetic loci, as shown in the present study.

[†]Frequency of the transgenic plants indicated in parentheses was confirmed by PCR.

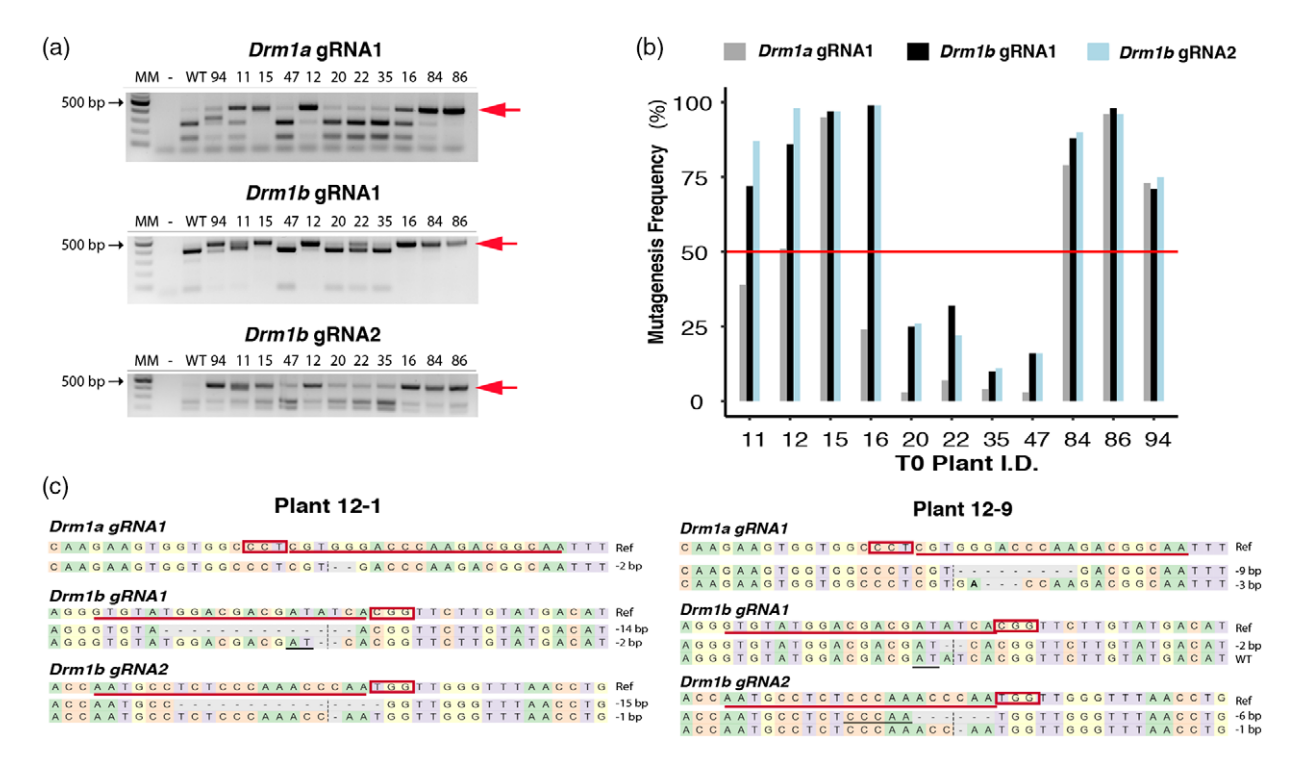


Figure 3. Characterization of mutations induced by the multiplex CRISPR/Cas9_Trex2 system in T0 and T1 plants. (a) Cleaved amplified polymorphic sequences (CAPS) genotyping assay. Eleven plants (numbered lanes) were genotyped by genomic PCR and the CAPS assay, with a 1-kb ladder, no genomic DNA control (—) and wild-type DNA control (WT). PCR amplicons (indicated by the red arrow heads) resistant to the enzyme digestion indicated the occurrence of mutations in the guide RNA (gRNA) targeted sites. (b) Mutagenesis frequency was determined for each T0 plant by next-generation sequencing. The threshold of the mutagenesis frequency at 50% is indicated by the red line. (c) Genotypes of transgene-free T1 plants in all targeted sites. Sequence alignment is shown between the wild-type reference sequences, indicated as Ref, and the mutant sequences from Plant 12-1 and 12-9. The gRNA targeted sites are highlighted by the red line with the protospacer adjacent motif (PAM) sequences indicated in the red boxes and the cleavage sites indicated by the vertical dotted lines. The deleted sequences are indicated by the dashed lines with the size of deletions indicated on the right. The microhomology sequences are highlighted by the black lines.

In summary, we have developed a protoplast-based assay to rapidly test and optimize the multiplex CRISPR/ Cas9 gene editing system in S. viridis. The mutagenesis frequency can be enhanced by co-expression with the Trex2 exonuclease, resulting in a unique mutation profile with larger deletions, no insertions and a high frequency of MMEJ repaired events. Furthermore, the optimized multiplex CRISPR/Cas9_Trex2 system can induce targeted mutagenesis in stable transgenic plants at remarkably high efficiency. This system allowed us to generate heritable knockouts in two tightly linked S. viridis genes from a small number of transgenic plants (10 T0 plants) in a timeframe as short as 3 months (starting from plant transformation to T1 seedlings). With the efficient Agrobacterium-mediated transformation method, this highly efficient pipeline makes it possible to create a large mutant collection of S. viridis in a rapid and high throughput manner. Moving forward, it would be interesting to test this CRISPR/Cas9_Trex2 system, or combinations of Trex2 with different Cas proteins, in other plants. These new systems have the potential to be widely applicable for achieving more predictable and deletion-only MMEJ-mediated mutations in many plant species.

Table 2 Summary of T1 plant characterization

	cterization o	·	Number of plants with mutations (frequency)		
T0 Plant I.D.	Number of T1 plants	Number of transgene- free T1	Drm1a (gRNA1)	Drm1b (gRNA1)	Drm1b (gRNA2)
12	10	5	5 (50%)	6 (60%)	3 (30%)
15	10	2	8 (80%)	8 (80%)	9 (90%)
84	10	2	8 (80%)	8 (80%)	9 (90%)
86	10	1	10 (100%)	9 (90%)	10 (100%)
94	10	0	7 (70%)	8 (80%)	10 (100%)

EXPERIMENTAL PROCEDURES

Plant materials, seed germination and plant growth conditions

Setaria viridis variety ME034v was used in the present study. To break dormancy and promote seedling germination, freshly harvested seeds were incubated at 29°C for 24 h in a 1.4 mm

Table 3 Summary of transgene-free T1 plant characterization

Genotype characterization of transgene-free T1 plants

Plant ID	Drm1a	<i>Drm1b</i> target 1	Drm1b target 2
12-1	Homozygous (-2 bp/-2 bp) [†]	Bi-allelic (-14 bp/ -2 bp) [†]	Bi-allelic (-15 bp/- 1 bp) [†]
12-9	Bi-allelic (-9 bp/- 3 bp) [†]	Heterozygous (-2 bp/WT) [†]	Bi-allelic (-6 bp/
12-15	WT [‡]	WT	WT
12-17	WT	WT	WT
12-22	WT	WT	WT
15-88	WT	WT	Heterozygous
15-95	WT	WT	Heterozygous
84-18	WT	WT	Heterozygous
84-27	WT	WT	WT
86-13	heterozygous	WT	Heterozygous

[†]Genotypes were confirmed by next-generation sequencing. The size of the deletion is indicated in parentheses.

gibberellic acid and 30 mm potassium nitrate solution (Sebastian et al., 2014). After 24 h of incubation, seeds were sterilized with 50% bleach for 10 min, followed by five water rinses and planted on germination media [0.5X MS, 0.5% sucrose, 0.4% Phytagel (Sigma, St Louis, USA), pH 5.7]. Seedlings were transplanted to soil 6 days after germination and grown under a 16:8 h light/dark photocycle at 26°C/22°C (day/night) and 30% relative humidity, comprising a protocol modified from Huang et al. (2019).

Guide RNA design and vector construction

The genomic sequences of each targeted gene were obtained by BLAST searching the S. viridis A10.1 reference genome from the phytozome database (https://phytozome.jgi.doe.gov). CRISPR gRNAs were designed to target exons in the 5' region of the gene or the conserved domains in each gene. The potential gRNA targeting sites were first identified using CRISPOR, and the first and second top-ranked sites were then selected based on their off-target potential and the presence of overlapping restriction enzyme sites (Haeussler et al., 2016). The targeted sequences were further verified by Sanger sequencing in the S. viridis variety ME034v. The conserved domains were identified by comparing the coding sequences from S. viridis with their orthologs from brachypodium, maize and Arabidopsis.

The gRNA constructs were made using the Golden Gate assembly method (Čermák et al., 2017). The backbone for the tRNAbased gRNA construct was pMOD_B2103, and the backbone of the Csy4-based gRNA construct was pMOD_B2303. The Cas9 constructs were pMOD_A1110 and pMOD_A1510. The Cas9_Trex2 construct, pMOD_A1910, was made by cloning the Trex2 coding sequence into the codon-optimized Cas9 expression cassette, based on the codon usage from wheat (Triticum aestivum). The GFP reporter constructs, pMOD_C3003 and pMOD_C3013, were made by cloning the GFP coding sequences under the control of the CmYLCV and PvUbi promoters with the 35S terminator. All of the constructs will be deposited to Addgene.

Protoplast isolation and transformation

Protoplast isolation and transformation were performed using a modified version of the polyethylene glycol (PEG)-mediated method (Li et al., 2016). In brief, leaves from 14-day young seedlings were sliced into small pieces with a razor blade and digested with the enzyme solution (1.5% cellulase, 0.75% Macerozyme; Kanematsu USA Inc., Chicago, IL, USA) for 4-5 h on a shaker at 40 rpm. The digested tissues were filtered through a 70-μM nylon filter (Fisher Scientific LLC, Pittsburgh, PA, USA) into W5 buffer (2 mm MES with pH 5.7, 154 mm NaCl, 125 mm CaCl₂, 5 mm KCl). Protoplasts were collected and resuspended in W5 buffer with gentle centrifugation at 100 g for 5 min. The number of protoplasts was estimated using a hemocytometer. Approximately 200 000 protoplasts were mixed with DNA plasmids (15 μ g per construct) in 20% PEG buffer and incubated at room temperature in the dark for 48 h. Transformation efficiencies were monitored by transforming protoplasts with a plasmid encoding GFP. Three transformation replicates were performed for each experiment. After 48 h of incubation, transformed protoplasts from all replicates were pooled to extract genomic DNA (Li et al., 2016).

T-DNA transformation and tissue culture

Agrobacterium tumefaciens-mediated transformation of S. viridis was performed as described previously with a few modifications (Van Eck et al., 2017). Callus initiation was first performed by removing the seed coats and sterilizing seeds with a 10% bleach plus 0.1% Tween solution for 5-10 min under gentle agitation. Seeds were plated on callus induction media with the embryos facing upward. The plates were placed at 24°C in the light for 1 week and then moved to dark for callus initiation. Embryogenic calli were collected after 4-7 weeks and inoculated with the AGL1 strain harboring the T-DNA construct. Inoculated calli were placed on co-culture medium and incubated in the dark at 20°C for 5-7 days. Transformed calli were transferred to the selection medium with 50 mg L⁻¹ hygromycin for 4 weeks at 24°C, then the selected calli were sub-cultured on plant regeneration media with 20 mg L^{-1} hygromycin under 16-h light to allow the growth of the transformed shoots. Elongated shoots were transferred to the rooting medium with 20 mg L⁻¹ hygromycin. To maximize the recovery of independent transformation events, when multiple shoots were regenerated from a single callus during selection, they were considered as one transformation event group. Only one shoot from each event group was transplanted to soil and grown to maturity. The transformation frequency was calculated as the total numbers of the event group divided by the total numbers of infected calli.

Genotyping and mutant identification

Mutant identification and characterization were performed using two methods: genomic PCR with restriction enzyme digestion (CAPS assay) and Illumina paired-end read amplicon sequencing (Illumina, San Diego, CA, USA) (NGS assay). PCR was performed with GoTag Green Master Mix (Promega Corp., Madison, WI, USA) in accordance with the manufacturer's instructions, with an annealing temperature of 58°C and an extension time of 1 min. Amplicons were then subjected to restriction enzyme digestion using an enzyme that overlaps with the CRISPR/Cas9 cleavage site. PCR amplicons made with the corresponding primers were subjected to Illumina paired-end read amplicon sequencing by Genewiz Inc. (South Plainfield, NJ, USA). The raw NGS reads were analyzed using CRISPRESSO2 (Clement et al., 2019).

^{*}WT, wild-type sequence without mutations.

T-DNA transgene detection was conducted using two methods: genomic PCR amplification of the hygromycin gene that is close to the T-DNA left border and a luciferase assay to detect the expression of the luciferase reporter gene that is next to the T-DNA right border. The luciferase assay procedure was conducted using the Bio-Glo™ Luciferase Assay System (Promega Corp.) in accordance with the manufacturer's instructions. All the primers used in the present study are listed in Table S5.

Characterization of mutation profiles

Mutations in the NGS reads were characterized into three categories: deletions, insertions and others (including substitutions and substitutions with insertions or deletions). The mutagenesis efficiency of each mutation type was estimated by dividing the total number of modified reads by the total number of reads. To minimize the problem caused by sequencing errors from NGS, mutation reads that only occurred once in the NGS data were not included in the calculation. To quantify the mutations derived from NHEJ or MMEJ repair pathways, each distinct deletion read was categorized into three separate sequences: (i) the left flanking sequence; (ii) the deleted sequence; and (iii) the right flanking sequence. Mutation reads were considered as MMEJ products when > 2 bp of homology was identified at the junction site between left and right flanking sequences. Mutation reads without microhomology sequences at the junction sites were classified as NHEJ events.

ACKNOWLEDGEMENTS

We thank all members of Voytas Lab and Zhang Lab for helpful discussions and feedback, as well as Meredith Song for assisting with the genomic DNA extractions, genotyping and caring for plants. FZ was supported by a startup fund (to FZ) from the College of Biological Sciences, University of Minnesota. DV, CS and MG were supported in part by grant DE-SC0018277 from the DOE. HZ was supported by the grant ZDYF2017017 from the key research and development project of Hainan. PZ, PC and NMS were supported in part by a grant from NSF (IOS-1802848). The University of Minnesota is part of a team supporting DARPA's LiSTENS Program.

CONFLICT OF INTEREST

The authors declare no conflict of interest.

AUTHOR CONTRIBUTIONS

NMS, DFV and FZ designed the study. TW, CW, XK, HZ, MEG and CGS performed the experiments. TW, PAC, ZP and FZ analyzed data and prepared the figures and tables. TW, NMS and FZ wrote manuscript. All authors revised the manuscript and approved the final draft submitted for publication.

SUPPORTING INFORMATION

Additional Supporting Information may be found in the online version of this article.

Figure \$1. Setaria viridis protoplast assay pipeline to test genome editing reagents. Following protoplast isolation from young leaves of 14-day-old plants, genome editing reagents can then be transformed into protoplasts to evaluate editing efficacy. At 48 hpt, genomic DNA from individual candidate plants is extracted, then subjected to cleaved amplified polymorphic sequences (CAPS)

and NGS analysis. The different levels of shading in the edited samples from the CAPS assay represent different levels of editing efficiencies in individual samples.

Figure S2. (A) The schematic structure of the GFP reporter plasmids used in the protoplast. The GFP coding sequence (green boxes) was driven by either the CmYLCV (plasmid ID pMOD_C3003) or the PvUbi2 promoter (plasmid ID pMOD_C3103) labeled as the gray boxes with the HSP terminator (red boxes). The illustration is not to scale. (B) Mesophyll protoplast cells isolated from young leaves and transformed with the GFP reporter plasmids, pMOD_C3003 and pMOD_C3013. GFP expression was assayed at 24 and 48 hpt. Scale bars (white bars) in each protoplast sample = 400 μm .

Figure S3. (A) The schematic structures of the plasmids for testing the Csy and tRNA-based gRNA processing systems. In the Csy4 system, the Cas9 expressing plasmid, pMOD_A1510, contained the Cys4 coding sequence (dark blue box) with the Cas9 coding sequence (blue box) separated by the P2A sequence (yellow box) under the ZmUbi promoter (grey box). The gRNA expressing plasmids, pTW003, pTW005, and pTW006, contained a single gRNA sequence (light blue box) flanked by the Csy4 recognition sites (purple boxes) under the control of the CmYLCV promoter and the 35S terminator (red box). In the tRNA system, the Cas9 expressing plasmid, pMOD A1110, contained only the Cas9 coding sequences driven by the ZmUbi promoter. The gRNA expression plasmids, pTW001, pTW002 and pTW004, contained a single gRNA sequence (light blue box) flanked by the tRNA sequences (light green boxes). (B) The schematic structures of the plasmids for the multiplexed Cas9 and Cas9_Trex2 systems. The plasmids, pMG198, pMG199, pMG201 and pMG202, were constructed to contain three components: the Cas9 or Cas9_Trex2 expression cassette, the tRNA-based multiplexing gRNA cassette and the GFP reporter. The illustration is not to scale.

Figure S4. Distribution of deletions spanning the 400 bp to 500 bp of the gRNA targeted regions induced by either Cas9 (red) and Cas9_Trex2 (blue). The deletion frequency was calculated by dividing the total number of deletions at each nucleotide by the total number of deletion reads.

Figure S5. Comparison of the size distribution from deletions induced by Cas9 or Cas9_Trex2. The number of reads for each deletion size was estimated for four gRNA sites from the Ms26 and Ms45 genes, respectively. The examples of MMEJ-mediated deletions are indicated by the black arrows.

Figure S6. Example of the MMEJ-mediated deletions. The CRISPR gRNA target sites are indicated by the black double lines, with the PAM sequences outlined by black boxes. The CRISPR/Cas9 cleavage sites are indicated by the red arrows. The microhomology sequences are underlined in the wild-type sequences, with the deleted sequences highlighted in red.

Figure S7. Model for DNA repair after a CRISPR/Cas9_Trex2-induced DSB. After Cas9 (light blue circles) binds the target genomic DNA and cleaves DNA creating a DSB, the *Trex2* protein (yellow circles) then resections the exposed DNA 3' to 5'. The resected DSBs are repaired by either MMEJ, as indicated by the heavy-weighted arrow heads, or the NHEJ pathway, as indicated by the light-weighted arrow heads. The gRNA targeted site is highlighted in red, with the 3-bp PAM sequence underlined in black. The microhomology sequences are indicated by the black boxes. The junction site in the MMEJ repaired sequence is indicated by the blue line, whereas the junction in the NHEJ repaired sequence is indicated by the vertical red line.

Figure S8. (A) The schematic structures of T-DNA binary plasmids for stable transgenesis. Each T-DNA plasmid contained three components: the Cas9_Trex2 expression cassette, the tRNA-based

multiplexing gRNA cassette and the luciferase reporter. Within each construct, pTW037, contained one gRNA targeting Drm1b, pTW044 contained one gRNA targeting Drm1a and one gRNA targeting Drm1b, and pTW045 contained one gRNA targeting Drm1a and two gRNAs targeting Drm1b. (B) Genomic PCR genotyping to detect the presence of the T-DNA in T0 plants. Two controls were included in this experiment: one without genomic DNA (indicated as H₂O) and the other with wild-type S. viridis genomic DNA (indi-

Figure S9. Genomic PCR genotyping of T0 plants with the CAPS assay. The samples from left to right are a 1-kb ladder, a no-genomic DNA control (indicated as H₂0), a control with wild-type genomic DNA (indicated as WT) and individual T0 samples. PCR amplicons (as indicated by the red arrow heads) resistant to the enzyme digestion indicated the occurrence of mutations in the targeted sites.

Figure \$10. Genomic PCR genotyping of T1 plants with the CAPS assay. The samples from left to right are a 1-kb ladder, no-genomic DNA control (H₂0) and wild-type genomic DNA control (WT). The remaining samples correspond to individual T1 plants.

Figure S11. Genomic PCR genotyping for segregation of the T-DNA transgenes in T1 plants. The samples from left to right are a 1-kb ladder, no-genomic DNA control (H₂0), and wild-type genomic DNA control (WT) and individual T1 samples. The weak DNA bands present in lanes 3, 50 and 52 probably resulted from DNA overflowed from the adjacent lanes. Lanes 3 and 50 represent the samples from transgene-free wild-type control plants. Lane 52 represents the sample from T1 plant 12-1. An absence of T-DNA from this plant was confirmed by the luciferase assay independently.

Figure S12. The luciferase assay for transgene-free plant screening. In this 24-well plate, each well contained the leaf samples collected from individual T1 plants. The plate layout was organized as A1 and A2, transgenic controls: A3, WT transgene-free plant; A4, 15-28; A5, 15-41; A6, 15-45; B1, 15-56; B2, 15-95; B3, 12-16; B4, 86-130; B5, 84-18; B6, 84-12; C1, 86-13; C2, 94-33; C3, 94-32; C4, 94-8; C5, 86-6; C6, 94-34; D1, 94-35; D2, 94-36; D3, 94-48; D4, 86-7; D5, 86-2; D6, 12-20. T1 plant samples without the luciferase activity, 15-95, 84-18 and 86-13 were highlighted by yellow circles.

Table S1. Summary of the targeted genes.

Table S2. Summary of next-generation sequencing reads for each targeted site.

Table S3. Summary of off-targeting analyses on MS26 gRNA 1 using NGS.

Table S4. Summary of T1 plant genotypes.

Table \$5. Summary of primer information.

OPEN RESEARCH BADGES





This article has earned an Open Materials badge for making publicly available the components of the research methodology needed to reproduce the reported procedure and analysis.

This article has earned an Open Data Badge for making publicly available the digitally shareable data necessary to reproduce the reported results.

REFERENCES

- Allen, F., Crepaldi, L., Alsinet, C. et al. (2018) Predicting the mutations generated by repair of Cas9-induced double-strand breaks. Nat. Biotechnol. 37.64-72
- Ata, H., Ekstrom, T.L., Martínez-Gálvez, G., Mann, C.M., Dvornikov, A.V., Schaefbauer, K.J., Ma, A.C., Dobbs, D., Clark, K.J., and Ekker, S.C. (2018) Robust activation of microhomology-mediated end joining for precision gene editing applications. PLoS Genet. 14, e1007652.

- Bae, S., Kweon, J., Kim, H.S. and Kim, J.-S. (2014) Microhomology-based choice of Cas9 nuclease target sites. Nat. Methods, 11(7), 705-706.
- Bennetzen, J.L., Schmutz, J., Wang, H. et al. (2012) Reference genome sequence of the model plant Setaria. Nat. Biotechnol. 30(6), 555-561.
- Brutnell, T.P., Wang, L., Swartwood, K., Goldschmidt, A., Jackson, D., Zhu, X.-G., Kellogg, E., and Van Eck, J. (2010) Setaria viridis: a model for C4 photosynthesis. Plant Cell, 22(8), 2537-2544.
- Čermák, T., Curtin, S.J., Gil-Humanes, J. et al. (2017) A multipurpose toolkit to enable advanced genome engineering in plants. Plant Cell, 29, 1196-1217.
- Chari, R., Mali, P., Moosburner, M. and Church, G.M. (2015) Unraveling CRISPR-Cas9 genome engineering parameters via a library-on-library approach. Nat. Methods, 12(9), 823-826.
- Chen, K., Wang, Y., Zhang, R., Zhang, H. and Gao, C. (2019) CRISPR/Cas genome editing and precision plant breeding in agriculture. Annu. Rev. Plant Biol. 70, 667-697.
- Clement, K., Rees, H., Canver, M.C. et al. (2019) CRISPResso2 provides accurate and rapid genome editing sequence analysis. Nat. Biotechnol. 37(3),
- Collier, R., Thomson, J.G. and Thilmony, R. (2018) 'A versatile and robust Agrobacterium-based gene stacking system generates high-quality transgenic Arabidopsis plants', Plant J. Wiley Online Library, 95(4), 573-583.
- Defelice, M.S. (2002) Green Foxtail, Setaria viridis (L.) P. Beauv, Weed technology: a journal of the Weed Science Society of America. Cambridge University Press, 16(1), 253-257.
- Haeussler, M., Schönig, K., Eckert, H. et al. (2016) Evaluation of off-target and on-target scoring algorithms and integration into the guide RNA selection tool CRISPOR. Genome Biol. 17(1), 148.
- Huang, P., Mamidi, S., Healey, A. et al. (2019) 'The Setaria viridis genome and diversity panel enables discovery of a novel domestication gene',
- Lata, C., Gupta, S. and Prasad, M. (2013) Foxtail millet: a model crop for genetic and genomic studies in bioenergy grasses. Crit. Rev. Biotechnol. **33**(3), 328–343.
- Li, J., Stoddard, T.J., Demorest, Z.L. et al. (2016) Multiplexed, targeted gene editing in Nicotiana benthamiana for glyco-engineering and monoclonal antibody production. Plant Biotechnol. J. Wiley Online Library, 14(2), 533-
- Mazur, D.J. and Perrino, F.W. (1999) Identification and Expression of the TREX1 and TREX2 cDNA Sequences Encoding Mammalian 3'→5' Exonucleases. J. Biol. Chem. 274(28), 19655-19660
- Meng, X., Yu, H., Zhang, Y., Zhuang, F., Song, X., Gao, S., Gao, C. and Li, J. (2017) Construction of a Genome-Wide Mutant Library in Rice Using CRISPR/Cas9. Molecular plant, 10(9), 1238-1241.
- Minkenberg, B., Wheatley, M. and Yang, Y. (2017) CRISPR/Cas9-enabled multiplex genome editing and its application. Prog. Mol. Biol. Transl. Sci. 149, 111-132.
- Nguyen, D.Q., Van Eck, J., Eamens, A.L. and Grof, C.P.L. (2020) Robust and reproducible Agrobacterium-mediated transformation system of the C4 genetic model species Setaria viridis. Front. Plant Sci. Front. 11, 281.
- Qi, Y., Zhang, Y., Zhang, F. et al. (2013) Increasing frequencies of site-specific mutagenesis and gene targeting in Arabidopsis by manipulating DNA repair pathways. Genome Res. 23(3), 547-554.
- Sebastian, J. Wong, M.K., Tang, E. and Dinneny, J.R. (2014) Methods to promote germination of dormant Setaria viridis Seeds. PLoS One, 9(4),
- Shiraki, T. and Kawakami, K. (2018) A tRNA-based multiplex sgRNA expression system in zebrafish and its application to generation of transgenic albino fish. Sci. Rep. 8(1).
- Taheri-Ghahfarokhi, A., Taylor, B.J.M., Nitsch, R. et al. (2018) Decoding non-random mutational signatures at Cas9 targeted sites. Nucleic Acids Res. 46(16), 8417-8434.
- Tsai, S.Q., Wyvekens, N., Khayter, C. et al. (2014) Dimeric CRISPR RNAguided Fokl nucleases for highly specific genome editing. Nat. Biotechnol. 32, 569-576.
- Van Eck, J., Swartwood, K., Pidgeon, K. and Maxson-Stein, K. (2017) Agrobacterium tumefaciens-Mediated Transformation of Setaria viridis. In Genetics and Genomics of Setaria. (Doust, A. and Diao, X., eds). Cham: Springer International Publishing, pp. 343-356.
- Van Eck, J. (2018) The status of Setaria viridis transformation: agrobacterium-mediated to floral dip. Front Plant Sci. 9, 652-656. https://doi.org/ 10.3389/fpls.2018.00652.

- Xie, K., Minkenberg, B. and Yang, Y. (2015) Boosting CRISPR/Cas9 multiplex editing capability with the endogenous tRNA-processing system. *Proc. Natl Acad. Sci.* 112(11), 3570–3575.
- Yin, K., Gao, C. and Qiu, J.-L. (2017) Progress and prospects in plant genome editing. *Nature Plants*, **3**, 17107.
- Zhu, C., Yang, J. and Shyu, C. (2017) Setaria comes of age: meeting report on the second international Setaria genetics conference. Front. Plant Sci. 8, 1562.